Metallophysics and Advanced Technologies
Металофіз. новітні технол.
Metallofiz. Noveishie Tekhnol.
2026, vol. 48, No. 5, pp. 463–481
https://doi.org/10.15407/mfint.48.05.0463
Reprints available directly from the publisher

PACS numbers: 61.05.cp, 61.66.Dk, 61.72.Dd, 61.72.Ff, 65.40.De, 81.20.Ev, 81.40.Ef

Influence of Annealing on the CTE of Sintered Al–Si–Ni and Al–TiC Materials

V. V. Kaverinskiy, G. A. Bagliuk, S. F. Kyryliuk, Z. P. Sukhenko, I. M. Kirian*, and O. D. Rud*

I. M. Frantsevych Institute for Problems in Materials Science, N.A.S. of Ukraine,
3 Omeljan Pritsak Str.,
UA-03142 Kyiv, Ukraine
**G. V. Kurdyumov Institute for Metal Physics, N.A.S. of Ukraine,*
36 Academician Vernadsky Blvd.,
UA-03142 Kyiv, Ukraine

This study investigates the effects of annealing and annealing temperature on the temperature-dependent coefficient of thermal expansion (CTE) for two advanced materials: sintered Al–Si–Ni alloy and Al–TiC composite with *in situ* synthesized carbide particles. The experiments reveal significant differences in the annealing impact on the CTE behaviour of these materials. For the Al–TiC composite, the CTE demonstrates an Arrhenius-type dependence on temperature, with annealing causing a consistent reduction in CTE across the studied temperature range. While the activation energy associated with the Arrhenius-type dependence remains unaffected largely, the pre-exponential factor is altered significantly, pointing to structural and microstructural transformations. XRD analysis confirms that increasing the annealing temperature decreases the crystallite size, particularly, in the carbide phase, that correlates with the observed CTE reduction. In contrast, the Al–Si–Ni alloy exhibits a more complex response to annealing. Annealing at 420°C increases slightly the CTE at higher measuring temperatures (> 100°C), while annealing at 550°C causes a notable rise in CTE at lower temperatures and leads to more stable, nearly linear temperature dependence.

Corresponding author: Oleksandr Dmytrovych Rud
E-mail: rud@imp.kiev.ua

Citation: V. V. Kaverinskiy, G. A. Bagliuk, S. F. Kyryliuk, Z. P. Sukhenko, I. M. Kirian, and O. D. Rud, Influence of Annealing on the CTE of Sintered Al–Si–Ni and Al–TiC Materials, *Metallofiz. Noveishie Tekhnol.*, **48**, No. 5: 463–481 (2026). DOI: 10.15407/mfint.48.05.0463

Crystallite size in the alloy increases with annealing, aligning with the observed rise in CTE. These findings highlight the critical role of microstructural changes induced by annealing in controlling the thermal-expansion properties of Al-based alloys. Understanding these mechanisms offers valuable insights for tailoring material performance in applications requiring precise thermal stability.

Key words: coefficient of thermal expansion, sintered aluminium alloys, aluminium-matrix composites, annealing, structure, crystallite size.

У дослідженні проаналізовано вплив температури відпалу на температурну залежність коефіцієнта термічного розширення (КТР) для двох сучасних матеріялів: спеченого стопу Al–Si–Ni та композиту Al–TiC з карбідними частинками, синтезованими *in situ*. Експерименти виявили значні відмінності у поведінці КТР цих матеріялів після відпалу. Для композиту Al–TiC КТР демонструє залежність від температури типу Арреніюсової, причому відпал спричиняє постійне пониження КТР у всьому дослідженому температурному діяпазоні. Хоча енергія активації, пов'язана із Арреніюсовою залежністю, залишається майже незмінною, значно змінюється передекспоненційний множник, що вказує на структурні та мікроструктурні трансформації. Аналіза за допомогою дифракції X-променів показала, що з підвищенням температури відпалу зменшується розмір кристалітів, особливо у карбідній фазі, що корелює зі спостережуваним пониженням КТР. Стоп Al–Si–Ni показав складнішу реакцію на відпал. Відпал за температури у 420°C незначно збільшив КТР за вищих температур міряння (> 100°C), тоді як відпал за 550°C спричинив помітне зростання КТР за нижчих температур і привів до стабільної, майже лінійної залежности КТР від температури. Розмір кристалітів у стопі збільшувався після відпалу, що узгоджується зі зростанням КТР. Ці результати підкреслюють ключову роль мікроструктурних змін, спричинених відпалом, у реґулюванні властивостей термічного розширення стопів на основі алюмінію. Розуміння цих механізмів дає змогу вдосконалювати матеріяли для застосувань, що потребують високої термічної стабільности.

Ключові слова: коефіцієнт теплового розширення, спечені алюмінійові стопи, алюмінійові матричні композити, відпал, структура, розмір кристалітів.

(Received 9 May, 2025; in final version, 15 October, 2025)

1. INTRODUCTION

The field of device construction, particularly for aerospace applications, necessitates lightweight materials with specific physical properties [1, 2]. One critical property is a coefficient of thermal expansion (CTE) compatible with materials such as steel and copper alloys. This compatibility is essential for orientation and navigation devices in flying objects, where dimensional instability can account for 20–50% of total device error [3]. Consequently, the development of lightweight

materials with low CTE values remains a pressing challenge in modern metallurgy and materials science.

Aluminium serves as the foundation for many lightweight materials due to its numerous advantages: low density (2700 kg/m^3), high corrosion resistance, excellent plasticity, affordability, non-toxicity, and ease of processing [4]. These properties often surpass those of other lightweight metals like magnesium, beryllium, or lithium. However, aluminium high linear thermal-expansion coefficient ($23.4 \cdot 10^{-6}\ K^{-1}$ in the 20–100°C range) [5] presents a significant drawback compared to materials like steel ($\cong 10–15 \cdot 10^{-6}\ K^{-1}$) [6] and copper ($16.8 \cdot 10^{-6}\ K^{-1}$) [7]. Therefore, reducing aluminium CTE through specialized alloying is crucial for its application in precision instrument making.

The Al–Si–Ni alloys, which contain 25–30% wt. silicon and 5–7% wt. nickel, exhibit CTE values comparable to steel. However, manufacturing homogenous Al–Si–Ni alloys with appropriate structures and properties poses significant challenges due to their broad solidification temperature range [8]. For example, an alloy with 30% wt. silicon and 7% wt. nickel has a liquidus temperature of ≅ 850°C and a solidus temperature of 557°C, as illustrated in Ref. [8]. During this interval, silicon and intermetallic compounds, known for their brittleness, tend to grow within the liquid phase, leading to phase segregation due to the difference in density. As a result, casting is unsuitable for these alloys, and production typically relies on powder metallurgy. This method involves pre-alloyed powders produced through rapid solidification, followed by solid-phase sintering and hot deformation processing [9]. Only this approach ensures a homogenous structure with fine silicon and Al_3Ni inclusions and acceptable mechanical properties [10].

As an alternative to Al–Si–Ni alloys, aluminium matrix composites (AMCs) are gaining attention. AMCs reinforced with ceramic particles exhibit superior strength, elastic modulus, and resistance to creep and fatigue compared to unreinforced aluminium. These properties make them highly attractive for the aerospace and automotive industries. In addition to improved strength, AMCs demonstrate enhanced hardness and wear resistance. Commonly used reinforcements include SiC, Al_2O_3, TiC, and TiB_2 [11–16]. Among these, Al–TiC composites stand out due to their excellent wear resistance, high strength-to-weight ratio, and mechanical properties. Moreover, the lattice parameters of TiC particles closely match those of solid aluminium, making them effective nucleation centres during the alloy crystallization [17, 18].

Several techniques are available for making particle-reinforced metal matrix composites (MMCs), ranging from casting [19, 20] to powder metallurgy (PM) methods [17, 20]. The segregation of reinforcement during solidification limits the performance of cast-route composites in various applications. Inhomogeneous distributions of the reinforcement have been widely reported to deteriorate mechanical

properties, particularly fatigue and fracture performance [19].

Al–TiC composites hold a key position among materials with low coefficients of thermal expansion, particularly for use in high-precision equipment and electronics. These composites are notable not only for their reduced CTE but also for their enhanced strength and hardness. Titanium carbide (TiC) forms exceptionally strong bonds with the aluminium matrix, making these materials resistant to mechanical deformation, even at elevated temperatures [21]. The presence of TiC particles limits the thermal expansion of the aluminium matrix while contributing to improved heat resistance. However, this comes at the expense of reduced plasticity, as the rigid TiC particles restrict the matrix's ability to deform under stress. Thanks to their high-temperature stability, Al–TiC composites are particularly suitable for demanding applications such as engine components and heat dissipation systems, where performance under high loads is critical.

The most common method for producing Al–TiC composites is powder metallurgy, which ensures a uniform distribution of TiC particles within the aluminium matrix. This process typically involves mixing aluminium and titanium carbide powders, followed by pressing and sintering in a vacuum or an inert gas environment, such as argon. Compared to traditional casting, powder metallurgy offers significant advantages, including minimized chemical reactions between the aluminium matrix and TiC reinforcement, as the synthesis occurs at lower temperatures [18]. However, a challenge with this approach is the poor wettability of titanium carbide particles by aluminium, often caused by oxide films on the TiC surface. This issue can limit the potential benefits of carbide reinforcement [22].

To overcome this limitation, alternative technologies have been developed, including the use of Al–Ti–C master alloys. These master alloys are created *via in situ* reactions in a mixture of elemental aluminium, titanium, and carbon powders, resulting in the formation of finely dispersed TiC particles within the aluminium matrix. This process occurs at relatively moderate temperatures (900–1000°C) [22–26], producing composites with improved properties.

One of the most promising techniques is *in situ* thermal synthesis, which ensures the formation of submicron-sized, spherical TiC particles that are well integrated into the aluminium matrix [27–29]. This method can avoid undesirable structural components formation, such as ternary carbides (MAX phases), intermetallics, or unreacted carbon residues. Figure 1 shows an isothermal section of the Al–Ti–C phase diagram at 900°C, calculated using the CALPHAD method [30, 31]. In this diagram, the marked narrow two-phase region that represents the Al–TiC equilibrium seems to be an ideal for thermal *in situ* synthesis of Al–TiC composites.

Studies [27, 28] have demonstrated that, when the aluminium con-

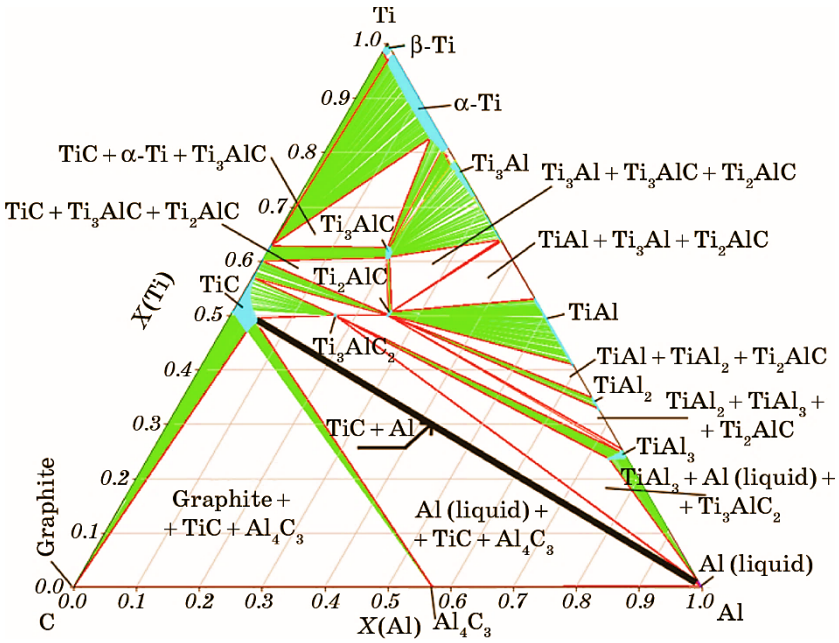

Fig. 1. Isothermal section of the calculated phase diagram of Al–Ti–C for 900°C [30].

tent exceeds 45%, the resulting TiC particles have roundish polyhedral submicron-sized shape, as shown in the micrograph in Fig. 2. These particles enhance the composite overall properties, making Al–TiC an ideal material for advanced applications.

Increasing the volume of carbides in the aluminium matrix is an effective way to lower the composite coefficient of thermal expansion. However, higher carbide content tends to increase porosity, which can adversely affect the composite mechanical properties [32]. In Al–TiC composites, the typical content of titanium carbide particles is limited to 10–15%. Beyond this range, the material plasticity decreases significantly, and its machinability becomes more challenging [33].

One promising solution to this issue is the application of additional hot stamping processes. This technique has been shown to reduce porosity, even at higher carbide concentrations, enabling the production of composites with exceptionally low CTE values (comparable to steel), while still retaining acceptable mechanical properties [28].

Despite significant advancements in the production and application of Al–TiC composites, their thermal expansion behaviour remains insufficiently studied. This is particularly true for their response to long-term high-temperature exposure, such as annealing. Similarly, for both Al–Si–Ni and Al–TiC composites, there is a lack of detailed

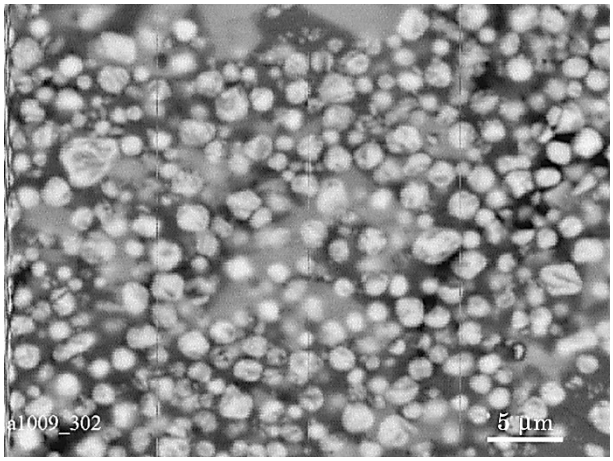

Fig. 2. Typical SEM image of the structure of *in situ* synthesized Al–TiC composite (45% Al) [27].

information regarding the impact of annealing on CTE values and how these values vary with temperature.

The present investigation aims to address this gap by exploring the relationship between annealing temperature and the CTE of these composites. This study seeks to provide new insights into the temperature-dependent behaviour of Al–TiC and Al–Si–Ni composites.

2. MATERIALS AND METHODS

The materials investigated in this study were an Al–Si–Ni sintered alloy and an Al–TiC composite, with their compositions summarized in Table 1.

Since the prior studies revealed that the Al–Si–Ni alloy production through merely mixing the does not achieve the desired mechanical properties and leads to a coarse structure even after hot stamping, prealloyed powder has been used [9]. The Al–Si–Ni alloy was prepared

TABLE 1. Compositions of the studied materials (% wt.). The composition of Al–TiC composite reflects the mass proportions of the initial materials for synthesis, corresponding to approximately 55% TiC by weight.

Al–Si–Ni sintered alloy	Al	Si	Ni
	65.8	28.5	5.7
Al–TiC composite	Al	Ti	C
	45	44	11

from powder of ground rapidly solidified ribbons produced using the melt-spinning technique. The ribbons with a thickness of 30–50 μm and a width of 9–12 mm were fabricated by casting molten material onto a rotating copper reel under controlled conditions, including a melt temperature of 1080°C, precise crucible pressure, and drum rotation speed. The process was conducted under a protective helium atmosphere using quartz crucibles at the G. V. Kurdyumov Institute for Metal Physics, N.A.S. of Ukraine [10].

The ribbons were mechanically ground in a Fritsch Pulverisette P-6 planetary ball mill to produce alloy powder. Grinding parameters included a rotation speed of 200 rpm, a ball-to-powder mass ratio of 10:1, and a grinding duration of 30 minutes with 12 steel balls (20 mm diameter) and approximately 37 g of powder. The resulting powder had an average particle size of 106 ± 5 μm, with particle sizes ranging from 4 to 381 μm.

Compaction of the Al–Si–Ni powders was achieved using a hydraulic press at pressures of 500–600 MPa. The powders were compacted into low-carbon steel capsules with external and internal diameters of 28 mm and 32 mm, respectively, and a total height of 37 mm (including the base and lid). These capsules optimized the deformation process and ensured uniform compression. Sintering was performed at 530°C for 2 hours, preceded by degassing at 350°C for 30 minutes. This temperature was selected to remain below the ternary eutectic point (540–550°C) for rapidly solidified materials with non-equilibrium phases, as noted in Ref. [3]. Solid-phase sintering was employed to prevent liquid-phase formation, which could lead to porosity and chemical distortion, as observed in earlier studies [10].

Hot deformation (forging) of the sintered samples was conducted at 520°C in a specially designed die. Before forging, the samples underwent additional lateral compression (20–30%) at the same temperature. After forging, the steel shells were removed by machining. The final samples exhibited no brittle fractures and were suitable for further processing.

Thermal synthesis of the Al–TiC master alloy followed the procedures detailed in Refs. [23, 27, 28]. Initial aluminium, titanium and carbon (graphite) powders mixtures has been blended in a barrel mixer with alcohol, pressed into briquettes at 500 MPa using a hydraulic press (GP60), and sintered in an argon-filled sealed chamber at 950°C using indirect induction heating. The sintered briquettes (spongy and porous because of TiC synthesis reaction) were subsequently crushed in a planetary mill for 5–15 minutes to achieve the desired particle size, with sieving used to ensure a maximum particle size of 10 μm. The obtained particles were polycrystalline aggregates of TiC crystals in aluminium matrix. The obtained powder was then pressed at 550 MPa into blanks measuring 40 mm in diameter and 12 mm in height. These

blanks were sintered in argon at 600°C for 1 hour and then subjected to hot stamping in a semi-closed die on an arc-stator press.

Post-stamping annealing was performed in a laboratory muffle furnace (SNOL 7.2/1300, ThermoLab) at 400°C, 500°C, and 600°C for the Al–TiC composite and at 420°C and 550°C for the Al–Si–Ni system material samples. The duration of the annealing for each case was 2 hours. Dilatometric measurements were carried out using a dilatometer with an inductive transducer. The error of CTE estimation on the final experimental curves was $\pm 0.3 \cdot 10^{-6}\,K^{-1}$. Microstructural analysis was conducted using an optical microscope (BH200M-RT) with digital micrographs captured using a SIGETA M3CMOS 32000 camera. The x-ray diffraction (XRD) study of the materials was carried out on a DRON-4 diffractometer with radiation MoK_α.

3. RESULTS AND DISCUSSION

3.1. Coefficient of Thermal-Extension Temperature Dependence

3.1.1. CTE of Sintered Al–Si–Ni Alloy

Figure 3 presents the temperature dependence of the studied Al–Si–Ni alloy CTE in temperature range of 50–300°C in its initial and annealed states. The studied samples were in the initial state and annealed at 420 and 550°C. From the provided plots, we can see that the CTE values of Al–Si–Ni alloy significantly increase with the temperature. For instance, in the initial state at 50°C its value is the lowest observed at

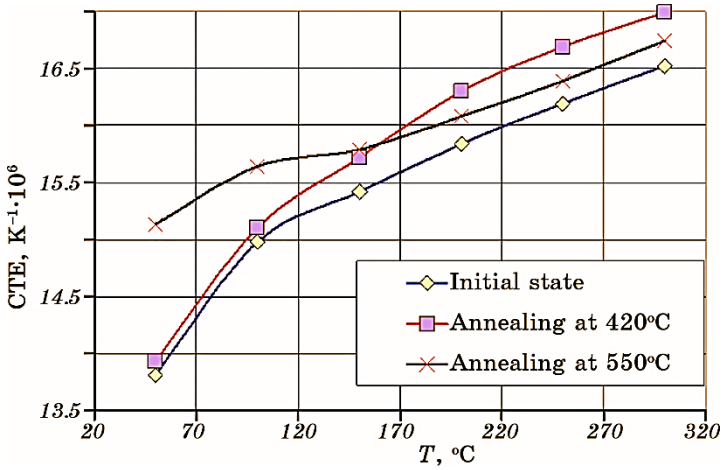

Fig. 3. Influence of annealing on the sintered Al–Si–Ni-alloy CTE temperature dependence.

$13.8 \cdot 10^{-6}\ K^{-1}$. However, at 300°C it rises to $16.5 \cdot 10^{-6}\ K^{-1}$. The growth is not linear, especially for not annealed and annealed at 420°C samples. A significant jump is observed in the range of 50–100°C.

Annealing at 420°C almost does not affect the material CTE at lower temperatures. The observed difference in the range of 50–150°C is comparable with the measurement accuracy. At higher temperatures, some slight but notable ($\cong 0.5 \cdot 10^{-6}\ K^{-1}$) increase of CTE for the annealed at 420°C specimen is observed. Annealing at 550°C leads to more significant growth of CTE at lower temperatures: for 50°C, the difference is of $1.3 \cdot 10^{-6}\ K^{-1}$, and for 100°C, it is of $0.66 \cdot 10^{-6}\ K^{-1}$. However, at temperatures higher than 200°C, the difference becomes insignificant and close to the measurement inaccuracy. It could be seen that, after annealing at 550°C, CTE of the material appears more stable—the mentioned jump at 50–100°C disappeared and its temperature dependence becomes almost linear and less pronounced.

Regarding the nature of the effect of annealing on the CTE, it can be assumed that annealing somehow affects the redistribution of the final mechanical stresses between the matrix and the silicon and intermetallic particles. Annealing can stabilize finely dispersed, in particular intermetallic, particles and prevent their agglomeration. When the particles remain evenly distributed and are not prone to coalescence, this contributes to an increase in the density of interphase boundaries, since each particle forms its boundary with the matrix. Annealing helps to eliminate residual stresses accumulated during the deformation of the composite. This relaxation contributes to the redistribution of particles at the microstructural level, where strong adhesion between the phases creates additional interphase boundaries.

3.1.2. CTE of Al–TiC Composite

The CTE temperature dependence of the Al–TiC composite was studied for the cases of annealing temperatures of 400, 500 and 600°C. CTE of the non-annealed samples has not been studied. The temperature dependencies of CTE values for the studied annealing temperatures are presented in Fig. 4.

From the presented results, it is evident that the CTE of the Al–TiC composite under consideration increases noticeably with a rise in temperature. Unlike the Al–Si–Ni system, annealing in this case significantly reduces the CTE. Furthermore, the observed reduction is relatively uniform across all temperatures. Increasing the annealing temperature further decreases the CTE.

The supposed reasons of the observed effect might be related to the relaxation of residual stress, dislocation density, changes in the morphology of particles or crystallite size caused by the annealing. Annealing, particularly, at higher temperatures, may lead to the redistribu-

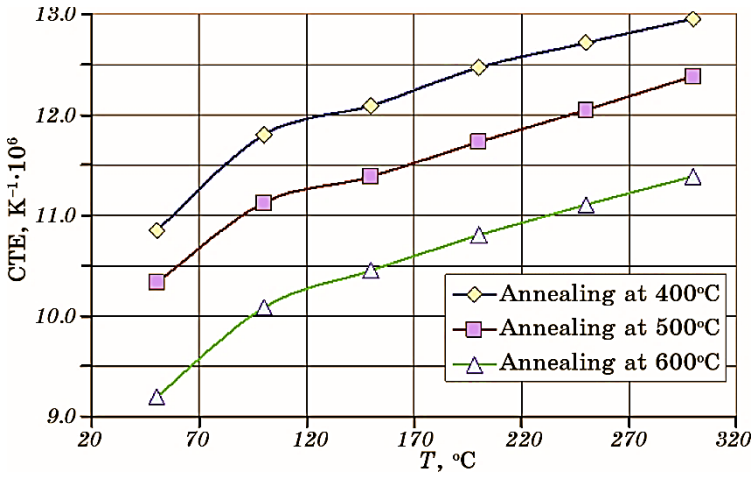

Fig. 4. Influence of annealing on the Al–TiC composite CTE temperature dependence.

tion of TiC particles within the matrix or changes in the density of interphase boundaries.

3.2. Microstructure of Composites

3.2.1. Sintered Al–Si–Ni Alloy

Microstructure photos of the initial and annealed material's samples are shown in Fig. 5. There is no notable difference in the material microstructure depending on the annealing temperature. In both presented cases are observed small almost eventually distributed silicon and intermetallic inclusions in the aluminium matrix. The shape of the inclusion is close to equiaxed polyhedra. The numerical characteristics of the microstructure are presented in Table 2, which includes average sizes of silicone and intermetallic inclusions and a number of all types

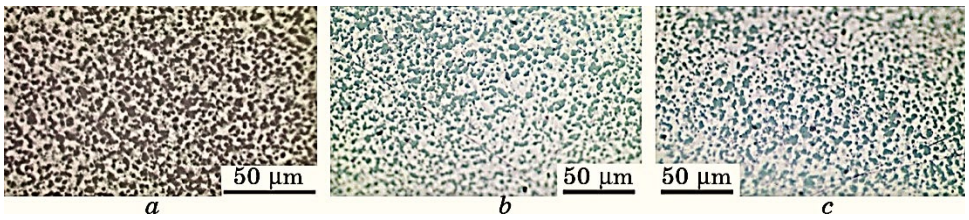

Fig. 5. Microstructure of the sintered Al–Si–Ni alloy after forging (*a*) and annealing at 420°C (*b*) and 550°C (*c*).

TABLE 2. Quantitative characteristics of the sintered Al–Si–Ni-alloy microstructure after different annealing temperatures.

Annealing temperature, °C	Average inclusions sizes, μm		Total number of the inclusions per 1 mm^2, $\times 10^4$
	Si	Al_3Ni	
Initial state	2.57 ± 0.13	1.43 ± 0.10	5.42 ± 0.86
420	2.77 ± 0.12	1.80 ± 0.07	4.05 ± 0.30
550	2.81 ± 0.09	1.82 ± 0.10	3.68 ± 0.20

of inclusions per 1 mm^2.

As can be seen in Table 2, some growth of the average inclusion sizes (both for silicon and for Al_3Ni) is observed after annealing at 420°C compared with the initial state. However, the difference in the measured values of the samples annealed at 420°C and 550°C is very slight and insignificant. Nevertheless, the difference between the number of inclusions per 1 mm^2, which seems to be a more reliable and precisely measured parameter, is rather different for all three studied cases. There is a decrease of this number after annealing and with razing its temperature. This may indicate some growth of the particles, gradual vanishing of the smallest ones, and growth in the distance between the inclusions. This seems to be a typical case of Ostwald's ripening, which accelerates with the temperature increasing.

Despite there being no direct evidence that the observed ripening of the inclusions when annealing effects directly the CTE of the material, it can be declared that those phenomena accompany each other, in this case—the particles ripen and CTE values increase when annealing and temperature growth.

3.2.2. Al–TiC Composite

Typical microstructure images (optical metallography) after annealing at different temperatures are shown in Fig. 6. The images demonstrate that the structure does not undergo radical changes under the influence of different annealing temperatures. Nevertheless, careful quantitative evaluation allows for the identification of even minor shifts in the structure.

The quantitative characteristics of the microstructure are presented in Table 3. The following parameters have been measured: the size of TiC particles (measured at ×500 magnification), the thickness of carbide cluster layers (measured at ×200 magnification), and the porosity estimation (carried out at ×50 magnification).

The measurement data indicate that the annealing temperature has almost no effect on the size of titanium carbide particles. The differ-

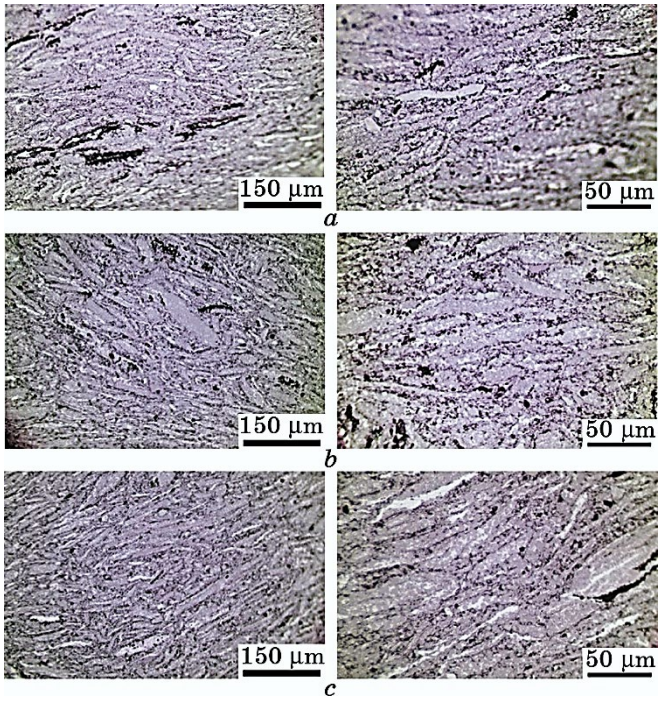

Fig. 6. Microstructure of the Al–TiC composite after stamping and annealing at following temperatures: 400°C (*a*), 500°C (*b*), 600°C (*c*).

TABLE 3. Quantitative characteristics of the Al–TiC-composite microstructure after different annealing temperatures.

Annealing temperature, °C	TiC particles average size, μm	Thickness of carbide cluster layers, μm	Porosity estimation, %
400	2.18 ± 0.11	7.83 ± 0.36	7.8 ± 1.4
500	2.33 ± 0.07	9.84 ± 0.37	4.6 ± 1.5
600	2.40 ± 0.08	11.96 ± 0.44	3.1 ± 0.9

ence in average values lies within the margin of statistical error. The size distribution of the particles follows a lognormal pattern, with no significant differences observed in the nature of the distribution.

The thickness of the carbide cluster layers observed in the structure changes only slightly with annealing temperature. A visual inspection of the microstructures reveals that in annealed at lower temperature samples, the carbide particles are more aggregated into clusters. With increasing annealing temperature, the particles become somewhat more separated, and more distinct matrix layers appear between them. It was also ob-

served that annealing reduces porosity in the material. Anyway, the influence of the annealing on the microstructure seems to be very slight.

3.3. X-Ray Diffraction Analysis

3.3.1. Sintered Al–Si–Ni Alloy

Observed by means of optical microscopy structural changes could only practically explain the possible reasons for CTE changes after a long-term thermal impact such as annealing. The x-ray diffraction (XRD) analysis is able to reveal more fine structure factors, among which are crystallite sizes and lattice parameters of the phases. An example of an XRD pattern for the studied material—a case of annealing at 420°C—is shown in Fig. 7. The present phases are typical and expected for the material, which are aluminium solid solution—the matrix, silicon and intermetallic compound Al_3Ni. The phase composition is qualitatively and quantitatively identical in each of the studied samples and is not affected by the annealing. Nevertheless, the XRD analysis reveals also the crystallite sizes and lattice parameters of the phases, as has been mentioned above. These results are presented in Table 4.

The given results show that this does not affect the lattice parameters of any phase presented in the material. However, there is a significant influence on the crystallite size both for matrix and for inclusions. The crystallite size of the aluminium matrix grew about 1.3 times after annealing at 420°C and more than 1.3 extra with the rise of the annealing to 550°C. Even more significant grows the crystallite size of silicon. For the Al_3Ni inclusions, however, only annealing at 550°C can af-

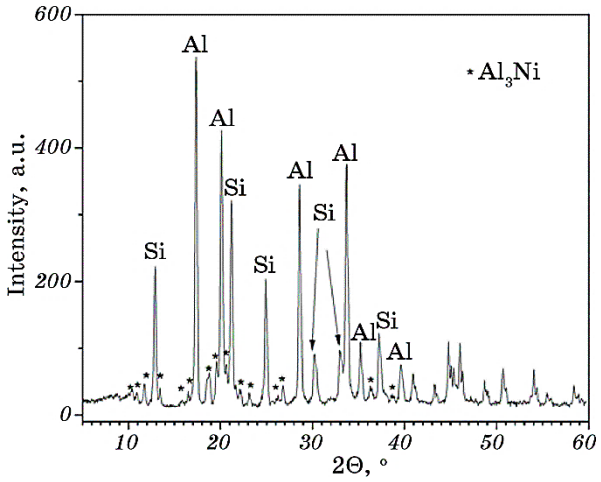

Fig. 7. Typical XRD pattern for the studied sintered Al–Si–Ni alloy.

TABLE 4. Effect of annealing temperature on the fine-structure characteristics of the phases present in the sintered Al–Si–Ni alloy according to XRD analysis.

Annealing temperature, °C	Phase	Lattice parameters, Å			Crystallite size, Å
		a	*b*	*c*	
Not annealed	Al	4.053	–	–	660
	Si	5.443	–	–	700
	Al_3Ni	6.602	7.382	4.811	450
420	Al	4.057	–	–	865
	Si	5.448	–	–	1150
	Al_3Ni	6.620	7.378	4.817	430
550	Al	4.059	–	–	1180
	Si	5.440	–	–	1800
	Al_3Ni	6.619	7.388	4.822	990

fect significantly its crystallite size, which increases more than twice.

Thus, for the studies here sintered Al–Si–Ni alloy annealing leads to both Ostwald ripening of the inclusions and growth of the crystallite size of matrix and inclusions. Moreover, the crystallite size of Al_3Ni starts to grow only at high annealing temperatures close to the solidus temperature. The observed structural changes could result in the mentioned CTE changes. It might be assumed that the Al_3Ni crystallite size increase, which appears at 550°C annealing, could be the reason for observed CTE rising at lower measuring temperatures. Moreover, it might be the phase most responsible for the annealing dependence of CTE for the material. The matrix and the silicon inclusions (their crystallite growth and ripening) could be responsible for more subtle changes in CTE temperature behaviour, which are the increase of CTE at higher temperatures after annealing at 420°C and its relative stabilization at the whole temperature range after annealing at 550°C.

3.3.2. Al–TiC Composite

The carried-out x-ray phase analysis has not shown any significant difference in the phase composition of the studied samples annealed at different temperatures. As you can see in the XRD pattern in Fig. 8, the only observed phases in the material are Al-based solid solution and TiC. The estimated part of TiC was about 55% wt.

The XRD also provides information on the lattice parameters and crystallite sizes for each of the present phases. The obtained results are presented in Table 5. In the XRD study, it was analysed as not annealed

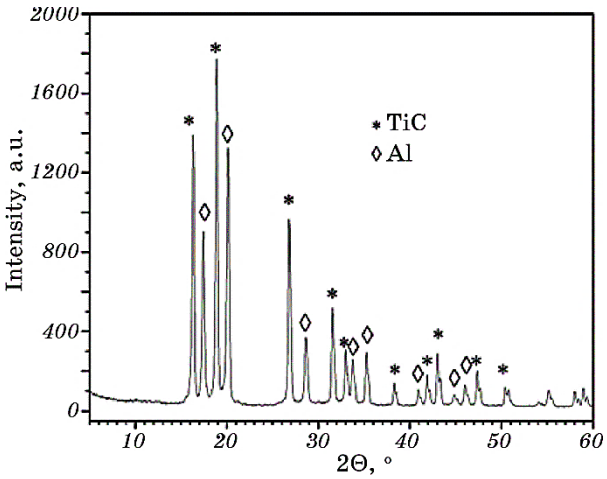

Fig. 8. XRD pattern for the studied Al–TiC composite.

TABLE 5. Effect of annealing temperature on the fine-structure characteristics of the phases present in the Al–TiC composite according to XRD analysis.

Annealing temperature, °C	Phase	Lattice parameter, Å	Crystallite size, Å
Not annealed	Al	4.0548	511
	TiC	4.3255	940
500	Al	4.0597	414
	TiC	4.3272	533
600	Al	4.0581	310
	TiC	4.3284	480

instead of annealed at 400°C. Others were the same.

We can see that annealing does not have any effect on the lattice parameters of any phase. However, the impact on the crystallite sizes is rather more valuable. It is notable that the annealing and its temperature rising lead not to growth but to a significant decrease of the crystallite sizes both for Al-based solid solution and for TiC. The annealing almost twice reduces its value for TiC. Rising annealing temperature from 500°C to 600°C has an additional 10% effect on the crystallite size of TiC declining.

Thus, for the studied material we observe that the CTE decreasing with the annealing temperature growth is clearly accompanied by the crystallite sizes decreasing both for the metal matrix and for the carbides. The observed relationship between decreasing CTE and reduced crystallite sizes is a realistic outcome of annealing. It might highlight

the complex interplay between microstructure evolution, defect dynamics, and interfacial phenomena in determining the thermal properties of a material.

3.4. Discussion

The relationship between annealing temperature, grain size, and the coefficient of thermal expansion in MMC is known and a well-documented phenomenon in materials science for different materials. Generally, as the grain size decreases, the CTE tends to increase due to the enhanced contribution of grain boundaries, which have different thermal expansion behaviours compared to the grain interiors. For example, in work [34], they studied the effects of grain size on the thermal expansion behaviour of the Fe–Ni invar alloy. The results showed a possibility of achieving different thermal expansion coefficients over a wide range of $(3.1–7.8)\cdot10^{-6}\ K^{-1}$ for the same alloy through grain size control. The thermal expansion difference between grain boundaries and crystallites was enlarged in the invar alloy.

However, in certain MMCs, increasing the annealing temperature can lead to a reduction in CTE. This effect is often attributed to the relaxation of residual stresses and changes in the microstructure, such as the redistribution of reinforcing particles like carbides within the metal matrix. For instance, in aluminium matrix composites reinforced with silicon carbide SiC and other particles, heat treatment has been shown to influence mechanical properties and thermal expansion [35]. Specifically, the CTE after treatment without reinforcement applied was reduced, while no significant difference was seen with reinforcement applied.

Additionally, the presence of reinforcing particles with a lower CTE than the metal matrix can lead to a mismatch in thermal expansion, inducing internal stresses that affect the overall CTE of the composite. The distribution and morphology of these particles, influenced by annealing, play a crucial role in determining the composite's thermal expansion behaviour [36].

The study [37] declares that, despite the known fact that the CTEs of alloys and composites are mainly changed by a volume fraction and shape of the second phases [38, 39], the CTE of particle-reinforced MMCs is affected by several other factors. These include: plasticity due to CTE mismatch between reinforcement and matrix, during heating or cooling; reinforcement fracture, residual stress, and local stresses at points of contact between reinforcement [40]. An incompressible plastic layer may form at the particle/matrix interface, and result in a lower expansion of the matrix, and thus, the overall composite [41]. The CTE of the composite is generally less than the rule of mixtures value because the presence of ceramic particles (usually of

low CTE) introduces a constraint on the expansion of the metallic matrix (usually of high CTE). In this regard, it is important to point out that interface can exert some influence on the value of CTE, especially, for very small particle sizes.

Thus, the observed here influence of annealing and its temperature on the Al-based MMCs' CTE and its relationship with the crystallite sizes does not contradict general concepts for such composites. Moreover, the obtained results significantly complement the insight into the thermal dependence of sintered Al–Si–Ni and Al–TiC materials CTE and the annealing effect on it observed at different temperature ranges.

It was shown that annealing could either increase or decrease the crystallite size, but lower crystallite size for the studied here composites often means the lower values of CTE. In the sintered Al–Si–Ni alloy, annealing and raising its temperatures results in crystallite size increasing and inclusions ripening that leads to CTE increase. A key role in this phenomenon can be played by Al_3Ni particles, the crystallite growth of which after high-temperature annealing can lead to an increase in the CTE at lower temperatures and its relative stabilization. On the other hand, the Al–TiC shows the contrary reaction on annealing—its crystallite decrease, which may lead to the observed CTE lowering.

4. CONCLUSIONS

An experimental investigation was carried out to study the influence of annealing and its temperature on the temperature dependence of the coefficient of thermal expansion for sintered Al–Si–Ni alloy and Al–TiC composite material containing *in situ* synthesized carbide particles.

The CTE of both materials increases with rising temperature. However, the effect of annealing on the sintered Al–Si–Ni alloy CTE differs from that observed in the Al–TiC composite. Annealing at a lower temperature (420°C) slightly increases the CTE at higher (> 100°C) measuring temperatures. In contrast, annealing near the solidus temperature (550°C) significantly raises the CTE at lower measuring temperatures, makes it more stable, and results in nearly linear temperature dependence.

Changes in CTE following annealing are accompanied by structural modulations. Notably, variations in crystallite size, determined through XRD analysis, were observed. A decrease in crystallite size correlates with a reduction in CTE for both materials. However, annealing affected crystallite size differently in the studied materials: in the sintered Al–Si–Ni alloy, annealing and increased temperature led to larger crystallites, whereas in the Al–TiC composite, higher annealing temperatures caused a reduction in crystallite size, particularly in the carbide phase. These differences in the effects of annealing on crystallite size are likely contributing factors to the contrasting CTE

behaviours of the two materials.

REFERENCES

1. O. E. Osintsev, *Met. Sci. Heat Treat.*, **40**: 172 (1998) (in Russian).
2. Z. Ahmad, *Aluminium Alloys: New Trends in Fabrication and Applications* (IntechOpen: 2012).
3. V. V. Vasenyev, *Razrabotka Kompozitsionnogo Materiala na Osnove Sistemy Al–Si–Ni s Nizkim Koeffitsientom Lineynogo Rasshireniya i Tekhnologii Izgotovleniya Izdeliya Raketno-Kosmicheskoy Tekhniki* [Development of a Composite Material Based on the Al–Si–Ni System with a Low Coefficient of Linear Expansion and Manufacturing Technology for Rocket and Space Equipment] (Thesis of Disser. for Dr. Techn. Sci.) (Moskva: 2017) (in Russian).
4. E. L. Rooy, *Introduction to Aluminum and Aluminum Alloys* (ASM International: 1990).
5. O. E. Osintsev and S. L. Nikitin, *Vysokoprochnyye Korrozionnostoykie Liteynyye Alyuminievyye Splavy Sistemy Al–Mg s Povyshennym Soderzhaniem Kremniya* [High-Strength, Corrosion-Resistant, Cast Aluminium Alloys of the Al–Mg System with Increased Silicon Content] (Moskva: MATI: 2008) (in Russian).
6. *Temperature Coefficient of Linear Expansion of Steel*
7. G. V. Samsonov, *Handbook of the Physicochemical Properties of the Elements* (Springer: 1968).
8. T. Bedo, B. Varga, D. Cristea, A. Nitoi, A. Gatto, E. Bassoli, G. Bulai, I.-L. Velicu, I. Ghiuta, S. Munteanu, M. A. Pop, C. Gabor, M. Cosnita, L. Parv, and D. Munteanu, *Metals*, **9**, Iss. 5: 483 (2019).
9. V. V. Kaverinsky, G. A. Bagliuk, S. F. Kyrylyuk, D. G. Verbylo, Z. P. Sukhenko, I. M. Kirian, M. A. Skoryk, and O. D. Rud, *Metallofiz. Noveishie Tekhnol.*, **47**, No. 3: 257 (2025).
10. G. A. Bagliuk, T. O. Monastyrska, V. V. Kaverinsky, V. P. Bevz, V. K. Nosenko, I. M. Kirian, D. L. Pakula, V. V. Kyrylchuk, A. M. Lakhnik, and O. D. Rud, *Metallofiz. Noveishie Tekhnol.*, **45**, No. 8: 951 (2023).
11. J. M. Torralba, C. E. da Costa, and F. Velasco, *J. Mater. Process. Technol.*, **133**: 203 (2003).
12. O. Beffort, S. Long, C. Cayron, J. Kuebler, and P.-A. Buffat, *Composites Sci. Technol.*, **67**, Iss. 3–4: 737 (2007).
13. I. Topcu, H. O. Gulsoy, N. Kadioglu, and A. N. Gulluoglu, *J. Alloys Compd.*, **482**: 516 (2009).
14. K. M. Shorowordi, T. Laoui, A. S. M. A. Haseeb, J. P. Celis, and L. Froyen, *J. Mater. Process. Technol.*, **142**, Iss. 3: 738 (2003).
15. J. C. Viala, M. Peronnet, F. Bosselet, and J. Bouix, *Proc. Int. Conf. Compos. Mater. (ICCM-12) (July 5–9, 1999, Paris)*.
16. P. Lü, X. Yue, H. Ru, and L. Yu, *Rare Metals*, **29**: 92 (2010).
17. X. C. Tong and A. K. Ghosh, *J. Mater. Sci.*, **36**: 4059 (2001).
18. S. Mohapatra, A. K. Chaubey, D. K. Mishra, and S. K. Singh, *J. Mater. Research Technol.*, **5**, Iss. 2: 117 (2016).
19. R. S. Rana, P. Rajesh, and S. Das, *Int. J. Sci. Eng. Res.*, **3**, No. 6: 1 (2012).
20. M. O. Shabani and A. Mazahery, *Ceram. Int.*, **39**, Iss. 2: 1351 (2013).

21. A. Onat, H. Akbulut, and F. Yilmaz, *J. Alloys Compd.*, **436**: 375 (2007).
22. C. Selcuk and A. R. Kennedy, *Mater. Lett.*, **60**: 3364 (2006).
23. Y. A. Shishkina, G. A. Bagliuk, A. A. Mamonova, and I. B. Tikhonova, *Powder Metall. Met. Ceram.*, **52**: 154 (2013).
24. M. S. Song, B. Huang, M. X. Zhang, and J. G. Li, *Int. J. Refractory Metals Hard Mater.*, **27**, Iss. 3: 584 (2009).
25. Q. C. Jiang, H. Y. Wang, Y. G. Zhao, and X. L. Li, *Mater. Res.*, **40**: 521 (2005).
26. X. Zhang, X. Zeng, S. Zeng, and Q. Li, *Trans. Nonferrous Met. Soc. China*, **6**: 114 (1996).
27. Y. A. Shishkina, G. A. Bagliuk, A. A. Mamonova, M. E. Holovkova, and Y. B. Tykhonova, *Ceram.: Sci. Life*, **31**, No. 2: 52 (2016) (in Ukrainian).
28. Y. O. Shishkina, G. A. Bagliuk, Y. S. Kyryliuk, S. F. Kyryliuk, O. V. Tolochyna, and V. M. Talash, *Mater. Sci.*, **59**: 679 (2024).
29. S. Purush and M. J. Koczak, *Mater. Sci. Eng. A*, **144**: 37 (1991).
30. V. V. Kaverinsky, G. A. Bagliuk, and Z. P. Sukhenko, *J. Mater. Eng. Perform.*, **33**: 9976 (2024).
31. *PyCALPHAD: Computational Thermodynamics*
32. M. N. Arif, M. Bukhari, D. Brabazon, and M. Hashmi, *IOP Conf. Ser.: Mater. Sci. Eng.*, **701**: 012057 (2019).
33. B. Harris, *Engineering Composite Materials* (London: The Institute of Materials: 1999).
34. Y. Liu, L. Liu, Z. Wu, J. Li, B. Shen, and W. Hu, *Scripta Mater.*, **63**, Iss. 4: 359 (2010).
35. K. Chattrakul, N. Sornsuwit, and P. Muangnoy, *Processes*, **12**: 2464 (2024).
36. O. Matvienko, O. Daneyko, T. Kovalevskaya, A. Khrustalyov, I. Zhukov, and A. Vorozhtsov, *Metals*, **11**, Iss. 2: 279 (2021).
37. B. Karthikeyan, S. Ramanathan, and V. Ramakrishnan, *Adv. Mater. Research*, **264–265**: 663 (2011).
38. S. J. Feltham, B. Yates, and R. J. Martin, *Mater. Sci.*, **17**: 2309 (1982).
39. C.-S. Park, C.-H. Kim, M.-H. Kim, and C. Lee, *Mater. Chem. Phys.*, **88**: 46 (2004).
40. N. Chawla and K. K. Chawla, *Metal Matrix Composites* (New York: Springer: 2006).
41. V. Ramakrishnan, A. Ramasamy, P. P. Gupta, and H. Murthy Narayana, *Proc. 16th National. Heat Mass Transf. Conf.* (Calcutta: 2002), p. 216.